HOKKAIDO UNIVERSITY

Title	Direct observation of subsurface charge ordering in Fe3O4(001) by scanning tunneling microscopy/spectroscopy
Author(s)	Hiura, Satoshi; Ikeuchi, Akira; Jochi, Masafumi et al.
Citation	Applied Physics Express (APEX), 10(4), 45701 https://doi.org/10.7567/APEX.10.045701
Issue Date	2017-04
Doc URL	https://hdl.handle.net/2115/68379
Rights	© 2017 The Japan Society of Applied Physics
Type	journal article
File Information	APEX_HokkaidoUniv_Hiura.pdf

Hokkaido University Collection of Scholarly and Academic Papers : HUSCAP

Direct observation of subsurface charge ordering in $Fe_3O_4(001)$ by scanning tunneling microscopy/spectroscopy

Satoshi Hiura*, Akira Ikeuchi, Masafumi Jochi, Riku Yamazaki, Sotaro Takahashi, Agus Subagyo, Akihiro Murayama and Kazuhisa Sueoka

Graduate School of Information Science and Technology, Hokkaido University, Sapporo 060-0814, Japan

In this study, we characterized $Fe_3O_4(001)$ films using scanning tunneling microscopy/spectroscopy (STM/STS). On the film surfaces, individual iron atoms and $(\sqrt{2}\times\sqrt{2})R45°$ reconstructed structures were observed by STM. The STS results showed the higher local density of states just below the Fermi level of narrow sections than wide ones of the surface reconstruction perpendicular to the iron rows. Periodical density of states modulations reproducing this electronic structure were clearly observed by the differential tunneling conductance map. These experimental results revealed the presence of subsurface charge ordering of Fe^{2+}-Fe^{2+} and Fe^{3+}-Fe^{3+} dimers, as proposed in previous density functional theory studies.

Magnetite (Fe_3O_4) is a magnetic iron oxide with unusual properties such as half-metallicity, a high Curie temperature of 858 K and a metal-insulator (Verwey) transition at 120 K in the bulk state.[1–3] The disappearance of half-metallicity and emergence of a Verwey transition on the surface of $Fe_3O_4(001)$ at room temperature have been reported previously.[4–9] Because of these properties and phenomena, Fe_3O_4 is a potential material for investigating electronic correlation effects in oxides. Investigations of the surface structural and electronic properties of Fe_3O_4 at the atomic scale are necessary for the development of future oxide-based devices.

The $Fe_3O_4(001)$ surface structure has been studied previously by scanning tunneling microscopy (STM) and low-energy electron diffraction (LEED).[10–12] A $(\sqrt{2}\times\sqrt{2})R45°$ surface reconstruction has often been observed on the $Fe_3O_4(001)$ surface. Several research groups have observed individual iron atoms in a B-plane (Fe_B) using STM, which revealed wavelike structures of the Fe_B rows along the [110] direction, as depicted in Fig. 1(a).[10–16] Pentcheva *et al*. predicted a B-terminated surface structure on the basis of density functional theory (DFT) calculations.[17,18] They suggested that the $(\sqrt{2}\times\sqrt{2})R45°$ reconstruction is a result of a Jahn–Teller distortion and that the surface exhibits a metallic nature. However, Jordan *et al*. reported a surface energy gap of ~0.2 eV on the basis of a scanning tunneling spectroscopy (STS) study,[19] which indicates a semiconducting nature of the surface. More recently, we revealed that the energy-gap value near the Fermi level of the surface Fe_B atoms is ~0.7 eV.[16] Moreover, the $(\sqrt{2}\times\sqrt{2})R45°$ surface reconstruction and the surface semiconducting nature have been proposed to be derived from the charge-ordered electronic states of the subsurface Fe_B atoms.[8,9,20] Figure 1(b) shows the proposed model of the subsurface charge-ordered structure. The Fe^{2+}-Fe^{2+} and Fe^{3+}-Fe^{3+} dimers aline in an alternating manner along the [1-10] direction in the subsurface layer. In the surface layer, the displacement of the Fe_B atoms produces inequivalent narrow "n" and wide "w" sections.[21,22] The inequivalent sections compose the $(\sqrt{2}\times\sqrt{2})R45°$ surface reconstruction pattern. Although a few theoretical studies have investigated subsurface electronic structures,[8,9] the literatures contain no related experimental studies. This experimental exploration can advance our understanding of not only the subsurface electronic structures but also the origin of the surface reconstruction and the surface semiconducting state.

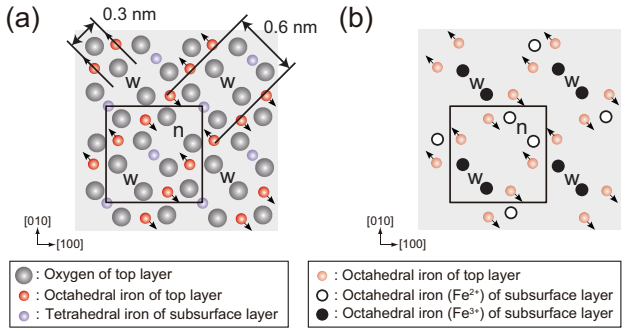

Fig. 1. Model of the B-terminated surface structure (a) and the subsurface charge-ordered structure (b) of $Fe_3O_4(001)$. The black arrows indicate the directions of the displacements of octahedral iron atoms of the top layer. The $(\sqrt{2}\times\sqrt{2})R45°$ reconstructed unit cell is indicated by the black square. The narrow and wide sections are marked as "n" and "w", respectively.

In this study, we used STM/STS to investigate the surface atomic structures and the subsurface electronic structures of $Fe_3O_4(001)$ films. The $(\sqrt{2}\times\sqrt{2})R45°$ reconstructed structure of the B-terminated surface was observed by STM at the atomic resolution. In addition, subsurface charge-ordered structures with alternating Fe^{2+}-Fe^{2+} and Fe^{3+}-Fe^{3+} dimers along the direction perpendicular to the rows were verified using STS spectra and differential tunneling conductance (dI/dV) maps. Notably, the two types of charge states of the subsurface Fe_B cations are labeled as Fe^{2+} and Fe^{3+}, however the valence charge of one of these cations is larger than the other by only $0.2e$.[8]

The experiments were carried out in an ultrahigh-vacuum system with a base pressure of 5×10^{-11} mbar. The system comprises two chambers, which contain measurement systems such as STM and molecular beam epitaxy apparatuses. STM/STS measurements were performed at room temperature using W-tips prepared by electrochemical etching. All STM images were acquired in the constant-current mode. A bias voltage was applied to the sample with respect to the grounded tip. STS measurements were performed with the

*E-mail address: hiura@nano.ist.hokudai.ac.jp

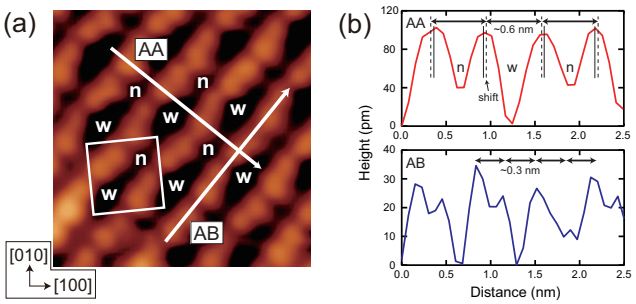

Fig. 2. (a) STM image (3.5×3.5 nm^2) of the Fe_3O_4(001) film surface. The STM image was taken with a W-tip at a set point of +1.0 V and 0.3 nA. The ($\sqrt{2}\times\sqrt{2}$)$R45°$ reconstructed unit cell is indicated by the white square. The narrow and wide sections are marked as "n" and "w", respectively. (b) Line profiles corresponding to the lines AA and AB in (a).

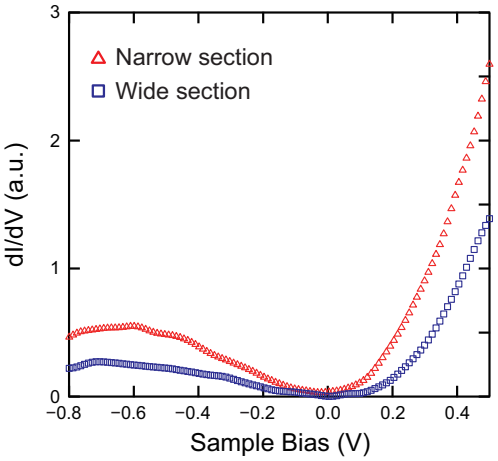

Fig. 3. dI/dV spectra obtained at the narrow and wide sections of the ($\sqrt{2}\times\sqrt{2}$)$R45°$ surface reconstruction perpendicular to the Fe_B rows. These spectra were obtained with a z-offset of 300 pm toward the surface with respect to the original set point of +1.2 V and 0.3 nA.

feedback loop turned off. The dI/dV signal was obtained using a standard lock-in technique with a modulation signal of 20 mV_{rms} at 5.24 kHz. The occupied state dI/dV image shown in Fig. 4(b) was acquired using the multipass scanning method.[23] In this method, surface topography was measured in the first pass. During the second pass, the acquired topographic trace was used to obtain tunneling current and dI/dV signals at a specific bias voltage. The distance offset for the second pass was 100 pm toward the surface with respect to the topography measured during the first pass.

The epitaxially grown Fe_3O_4(001) films were prepared on MgO(001) single-crystal substrates by the deposition of Fe in the presence of oxygen.[13,14,16,22] The MgO(001) substrates were cleaned *in situ* by heating at 573 K for 16 h and were then annealed at 1073 K for 1 h under an oxygen atmosphere (7×10^{-7} mbar). The Fe deposition was performed using an electron-beam heating evaporator at a substrate temperature of 573 K. During film formation, the oxygen pressure was set in the range 7×10^{-7} to 1×10^{-6} mbar. The growth rate was 0.9 ML/min and film thickness was 20 nm. After the deposition, the grown films were post-annealed at 573 K for 30 min under the same oxygen pressure.

Figure 2(a) shows a constant-current STM image of the Fe_3O_4(001) film surface. This STM image was taken at a tunneling current of 0.3 nA and a bias voltage of +1.0 V. In Fig. 2(a), atomic rows with a ($\sqrt{2}\times\sqrt{2}$)$R45°$ symmetry (marked with the white square) are oriented along the [110] direction. As evident in the line profile AA in Fig. 2(b), the average distance between neighboring rows is ~0.6 nm. The STM image and line profile AA also indicate that the atoms within each row are slightly shifted along the direction perpendicular to the rows. This image and profile clearly demonstrate the presence of narrow and wide sections, as shown in Fig. 1. These small displacements of the atoms perpendicular to the rows have been observed previously in DFT and LEED analysis studies.[11,12,17,18] Within the rows, the average distance between neighboring atoms is ~0.3 nm (see the line profile AB in Fig. 2(b)). Because these shifts and the periodicities of the atoms correspond to those of the Fe_B atoms in the B-terminated Fe_3O_4(001) surface, as shown in Fig. 1(a), the atoms observed in the STM images should represent single Fe_B atoms in the B-plane.

We performed STS measurements on the Fe_3O_4(001) film surface to explore the subsurface electronic structures. Figure 3 shows two dI/dV spectra obtained at the previously described narrow and wide sections, in which subsurface Fe_B atoms are located, as shown in Fig. 1(b). These spectra were obtained with a z-offset of 300 pm toward the surface with respect to the original set point of +1.2 V and 0.3 nA so that the subsurface electronic states could be effectively detected. This STS result shows the higher local density of states (LDOS) just below the Fermi level of the narrow section relative to the wide one. These dI/dV signals may include contributions from the surface Fe_B atoms, however all surface Fe_B atoms exclusively exhibited an Fe^{3+} charge state.[4,9,16,20,24] If the spectra included mainly the surface Fe_B LDOS, such a visible difference in the LDOS would not be observed. Therefore, the dI/dV spectra in Fig. 3 should include mainly the subsurface electronic states.

We also performed dI/dV mapping of the Fe_3O_4(001) film surface to further elucidate the subsurface electronic structure. Figure 4(a) and (b) display a set of images acquired using the previously described multipass scanning method.[23] The STM (Fig. 4(a)) and dI/dV (Fig. 4(b)) images were obtained at a bias voltage of +1.0 V and –0.4 V, respectively. Figure 4(c) shows cross-sectional line profiles of the STM and dI/dV images taken along the arrows marked as X and Y, respectively. The relative positions of the arrows are the same. In the STM image, the Fe_B rows run along the [110] direction. However, the dI/dV image shows a periodical electronic structure that differs from that in the STM image. It comprises two different dI/dV peak intensities (high peak and low peak), as indicated by the line profile Y in Fig. 4(c). The line profile was taken along the [1-10] direction, i.e., the direction perpendicular to the Fe_B rows. This result indicates that the periodicities of high(low)-peak to high(low)-peak and high(low)-peak to low(high)-peak are ~1.2 and ~0.6 nm, respectively.

In the dI/dV image shown in Fig. 4(b), periodical patterns with a ($\sqrt{2}\times\sqrt{2}$)$R45°$ symmetry are clearly observed, as indicated by the white square. Two types of bright spots in the dI/dV image are observed between the Fe_B rows (see Fig. 4(a) and (b)). As evident in Fig. 4(c), the positions of high(low) peaks correspond to those of the narrow(wide) section, which is in good agreement with the dI/dV spectra

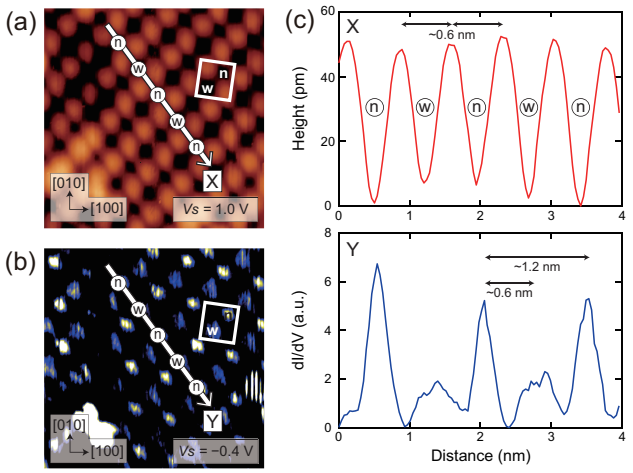

Fig. 4. (a), (b) Two-pass scan images (5.0×5.0 nm^2). First, an unoccupied-state STM image (a) was taken at a set point of +1.0 V and 0.3 nA. Second, a dI/dV image (b) was taken at a bias voltage of –0.4 V (the topography recorded in (a) was played with a z-offset of 100 pm toward the surface). The narrow and wide sections are marked as "n" and "w", respectively. (c) Line profiles taken along the arrows marked as X and Y in (a) and (b), respectively.

shown in Fig. 3. The observed dI/dV peaks are derived from the electronic states of surface oxygen atoms or subsurface Fe_B atoms (see the model in Fig. 1). Given that DFT calculations have predicted that the LDOS of surface oxygen atoms is almost zero near the Fermi level[9] and that the LDOS at –0.4 eV of subsurface Fe^{2+} cations is much higher than that of subsurface Fe^{3+} cations,[8,9] the high(low) peak should indicate the presence of Fe^{2+}-Fe^{2+}(Fe^{3+}-Fe^{3+}) dimers in the subsurface layer. These experimental findings clearly demonstrate the presence of subsurface charge ordering, and the subsurface charge-ordered electronic structure is sufficient to explain the $(\sqrt{2} \times \sqrt{2})R45°$ surface reconstruction.[8] Moreover, our results indicate that a degree of electronic ordering on the $Fe_3O_4(001)$ surface observed in previously reported STM images[25,26] likely corresponds to that on the subsurface, as described in this paper. Although the imaging mechanism of the subsurface electronic states has not been clarified completely, we suggest that the subsurface Fe_B atoms can be imaged on the basis of the insulating-like nature of the topmost $Fe_3O_4(001)$ surface, where the energy gap of ~0.7 eV is present near the Fermi level.[16]

In summary, we used STM/STS to investigate the surface atomic structures and the subsurface electronic structures of $Fe_3O_4(001)$ films. Individual Fe_B atoms and a B-terminated surface structure with a $(\sqrt{2} \times \sqrt{2})R45°$ symmetry were resolved using STM. The observed surface structure corresponds to the theoretical model reported by Pentcheva *et al.*[17,18] and to previously reported STM results.[10–12] Our STS spectra and dI/dV map experimentally revealed the presence of charge ordering in the $Fe_3O_4(001)$ subsurface layer. The charge-ordered electronic structure with two alternating types of LDOS exhibits a $(\sqrt{2} \times \sqrt{2})R45°$ symmetry and is in good agreement with the model of subsurface charge ordering.[8,9] These experimental findings clearly demonstrate that the subsurface Fe_B atoms show charge ordering of Fe^{2+}-Fe^{2+} and Fe^{3+}-Fe^{3+} dimers, which is responsible for the $(\sqrt{2} \times \sqrt{2})R45°$ surface reconstruction.

Acknowledgments

This work was supported by a Grant-in-Aid for JSPS Fellows (JSPS KAKENHI Grant Number 16J00053) and was partially supported by a Grant-in-Aid for Scientific Research S (JSPS KAKENHI Grant Number 16H06359).

1) E. J. W. Verwey, Nature **144**, 327 (1939).
2) A. Yanase and K. Siratori, J. Phys. Soc. Jpn. **53**, 312 (1984).
3) A. Yanase and N. Hamada, J. Phys. Soc. Jpn. **68**, 1607 (1999).
4) G. S. Parkinson, N. Mulakaluri, Y. Losovyj, P. Jacobson, R. Pentcheva, and U. Diebold, Phys. Rev. B **82**, 125413 (2010).
5) M. Kurahashi, X. Sun, and Y. Yamauchi, Phys. Rev. B **81**, 193402 (2010).
6) A. Pratt, M. Kurahashi, X. Sun, and Y. Yamauchi, J. Phys. D: Appl. Phys. **44**, 064010 (2011).
7) A. Pratt, M. Kurahashi, X. Sun, D. Gilks, and Y. Yamauchi, Phys. Rev. B **85**, 180409 (2012).
8) Z. Łodziana, Phys. Rev. Lett. **99**, 206402 (2007).
9) I. Bernal-Villamil and S. Gallego, J. Phys.: Condens. Matter **27**, 012001 (2015).
10) B. Stanka, W. Hebenstreit, U. Diebold, and S. A. Chambers, Surf. Sci. **448**, 49 (2000).
11) M. Fonin, R. Pentcheva, Y. S. Dedkov, M. Sperlich, D. V. Vyalikh, M. Scheffler, U. Rüdiger, and G. Güntherodt, Phys. Rev. B **72**, 104436 (2005).
12) M. Fonin, Y. S. Dedkov, R. Pentcheva, U. Rüdiger, and G. Güntherodt, J. Phys.: Condens. Matter **19**, 315217 (2007).
13) A. Subagyo, Y. Sasaki, H. Oka, and K. Sueoka, Phys. Status Solidi B **244**, 4482 (2007).
14) A. Ikeuchi, S. Hiura, T. Mizuno, E. Kaji, A. Subagyo, and K. Sueoka, Jpn. J. Appl. Phys. **51**, 08KB02 (2012).
15) S. Hiura, A. Ikeuchi, S. Shirini, A. Subagyo, and K. Sueoka, e-J. Surf. Sci. Nanotech. **12**, 26 (2014).
16) S. Hiura, A. Ikeuchi, S. Shirini, A. Subagyo, and K. Sueoka, Phys. Rev. B **91**, 205411 (2015).
17) R. Pentcheva, F. Wendler, H. L. Meyerheim, W. Moritz, N. Jedrecy, and M. Scheffler, Phys. Rev. Lett. **94**, 126101 (2005).
18) R. Pentcheva, W. Moritz, J. Rundgren, S. Frank, D. Schrupp, and M. Scheffler, Surf. Sci. **602**, 1299 (2008).
19) K. Jordan, A. Cazacu, G. Manai, S. F. Ceballos, S. Murphy, and I. V. Shvets, Phys. Rev. B **74**, 085416 (2006).
20) G. S. Parkinson, T. A. Manz, Z. Novotný, P. T. Sprunger, R. L. Kurtz, M. Schmid, D. S. Sholl, and U. Diebold, Phys. Rev. B **85**, 195450 (2012).
21) G. S. Parkinson, Z. Novotný, P. Jacobson, M. Schmid, and U. Diebold, J. Am. Chem. Soc. **133**, 12650 (2011).
22) S. Hiura, A. Ikeuchi, S. Shirini, A. Subagyo, and K. Sueoka, Jpn. J. Appl. Phys. **54**, 08LB02 (2015).
23) N. Ishida, M. Jo, T. Mano, Y. Sakuma, T. Noda, and D. Fujita, Nanoscale **7**, 16773 (2015).
24) Z. Novotny, N. Mulakaluri, Z. Edes, M. Schmid, R. Pentcheva, U. Diebold, and G. S. Parkinson, Phys. Rev. B **87**, 195410 (2013).
25) G. Mariotto, S. Murphy, and I. V. Shvets, Phys. Rev. B **66**, 245426 (2002).
26) I. V. Shvets, G. Mariotto, K. Jordan, N. Berdunov, R. Kantor, and S. Murphy, Phys. Rev. B **70**, 155406 (2004).